JOURNAL OF NANO- AND ELECTRONIC PHYSICS
Vol. **15** No 4, 04035(6pp) (2023)

ЖУРНАЛ НАНО- ТА ЕЛЕКТРОННОЇ ФІЗИКИ
Том **15** № 4, 04035(6cc) (2023)

Surface Laser Melting of a Carburized LPBF-Manufactured Ti-based Biomedical Grade Alloy

B.V. Efremenko[1], Yu.G. Chabak[1,2], E.V. Tsvetkova[1], A.V. Dzherenova[1], V.G. Efremenko[1,2], F. Kromka[2], V.I. Zurnadzhy[1,2], I.M. Olejnik[1]

[1] *Pryazovskyi State Technical University, 87555 Mariupol, Ukraine*
[2] *Institute of Materials Research, Slovak Academy of Sciences, 04001 Kosice, Slovakia*

(Received 25 May 2023; revised manuscript received 20 August 2023; published online 30 August 2023)

The object of this work is a study of the microstructure and hardness evolution of LPBF-manufactured biomedical alloy Ti-6Al-4V superficially modified by pack carburization and subsequent laser melting. Carburization was conducted in a powder of $(NH_2)_2CO$ (20 vol. %), $K_4Fe(CN)_6$ (20 vol. %), and a carbon black (60 vol. %) at 1000 °C (7 hours). The laser processing was fulfilled by fiber laser «TruFiber 400» (TRUMPF) of 1064 nm wavelength with a power of 400 W and scanning velocity of 5 mm·sec^{-1}. The investigations included optical (GX71 OLYMPUS) and scanning electron microscopy observations (JSM-7000F JEOL), energy-dispersive X-ray spectroscopy (INCAx-sight, Oxford Instruments), X-ray diffraction (X'Pert PRO, PANalytical, Cu-Kα radiation) and microhardness measurement (LM700AT LECO, under the load of 0.05 kg). It was found that carburization resulted in a 440-700 μm deep carbon-rich layer of αTi with an upper thin layer comprising TiC, TiO_2, and Al_2O_3. Carburization led to 720 ± 12 HV in a near-surface layer which is two times the bulk structure (322 ± 32 HV). A consequent laser scanning formed a 60-120 μm wide melted layer followed by the heat-affected zone (having a needle-like αTi-martensite) extended to ~ 0.8 mm depth. The melted layer had a fine-grained structure which included the dispersive particles of an oxycarbide $Ti(O_{0.8}C_{0.2})$ of both grainy and dendrite-like shapes. Consequently, the hardness of the melted layer rose up to 1000-1200 HV with a further gradual decrease, according to the declining carbon content profile. Laser melting was accompanied by cracks and shrinkage cavities formation. It also led to an increased roughness of the surface caused by its boiling under the laser melting.

Keywords: Ti-based biomedical alloy, Carburizing, Laser melting, Microstructure, Microhardness.

DOI: 10.21272/jnep.15(4).04035 PACS numbers: 42.62.Cf, 62.20.Qp, 61.66.Dk, 64.70.Kb

1. INTRODUCTION

Titanium alloy is traditionally used in medicine due to its unique properties, which combine exceptional biocompatibility, high corrosion resistance, low specific weight, and sufficiently high structural strength [1]. The prospects for the use of titanium alloys in medicine are growing taking into account the active development of additive technologies for biomedical components prototyping [2, 3]. The main drawback that limits the use of titanium alloys as joint implants is their low wear resistance when rubbing against metal surfaces. In this regard, research is being carried out aimed at improving the wear resistance of titanium alloys through surface hardening and protective coatings deposition. Various methods of surface engineering are used for this purpose, including PVD [4], DLC coating [5], electric-spark deposition [6], high-frequency work hardening [7], ions bombarding [8], thermal substrate deposition [9] and many others.

Among these methods, there is the traditional chemical-heat treatment focused on the diffusion saturation of titanium alloys with carbon or nitrogen [10]. It allows forming of a superficial titanium cermet (TiC-based) with improved hardness, fracture toughness, and nanoindentation plasticity [11]. As reported by Duan et. al [12], the solid carburization of Ti-6Al-4V alloy and $(TiB + La_2O_3)$/Ti composite allows getting the TiC reinforcements and Ti-C solid solutions which enhance the properties of these materials. The solid carburization of titanium alloy by contacting with grey cast iron is proposed in [13]. Employing the plasma glow shortens the process of carbonizing of Ti-6Al-4V alloy at 950 °C leading to "$TiC(V_8C_7) + \alpha$-Ti" structure with maximum hardness after 3 h holding [14, 15].

The laser treatment is acknowledged as a promising approach for different engineering applications [16]. Combining laser processing with other surfacing techniques may be a perspective for the improvement of the mechanical and wear behaviors of different metallic materials [17]. Combining the carburizing with a laser treatment regarding the Ti-based alloys remains not studied yet. Therefore this issue was the focus of the present work dedicated to the chemical/structural surface modification of the biomedical Ti-6Al-4V alloy by consecutive using solid carburization and laser melting.

2. MATERIALS AND METHODS

Ti-6Al-4V biomedical alloy specimens of 5 × 10 × 25 mm in size were fabricated by LPBF process using a "ProX DMP 320" (3D Systems) equipment with a 500 W fibre laser (1070 nm wavelength, 0.5 mm beam diameter). The powder feedstock (particle size is 39 ± 3 μm) was an EOS Titanium Ti64ELI powder of nominal chemical composition (wt. %): Al (5.5-6.75), V (3.5-4.5), O < 0.2, N < 0.05, C < 0.08, H < 0.015, Fe < 0.3, Ti – balance.

The surface of the specimens was ground to R_z = 0.2 μm and cleaned with ethanol. Then they were subjected to pack carburizing in the powder mixture consisting of $(NH_2)_2CO$ (20 vol. %), $K_4Fe(CN)_6$ (20 vol. %), and a carbon black (60 vol. %). The

specimens were carburized in a tightly closed box at 1000 °C for 7 hours. After duration completion, the box was slowly cooled inside the switched-off furnace. The carburized specimens were then laser processed using the fiber laser «TruFiber 400» (TRUMPF) (1064 nm wavelength). The process parameters were as follows: (a) the laser beam power – 400 W, (b) the laser beam spot diameter – 1.3 mm, (c) scanning velocity – 5 mm·sec^{-1}, (d) the tracks overlapping – 50 %, (e) focus distance – 20 mm, (f) environment – open air. This regime provided the surface melting of the specimen. After the process completion, the specimen was air-cooled to the ambient temperature.

The specimens were polished in a cross-section direction and etched with a Kroll solution (3 ml HF, 10 ml HNO_3, 87 ml H_2O). The microstructure was observed using optical microscopy GX71 (OLYMPUS) and scanning electron microscopy JSM-7000F (JEOL) equipped with energy-dispersive spectroscopy analyzer INCAx-sight (Oxford Instruments). The diffractometer X'Pert PRO (PANalytical) with Cu-Kα radiation was used for X-ray diffraction (the working parameters; voltage – 40 kV, current – 50 mA, scanning step – 0.03342 degree, scanning velocity – 0.0689 degree·sec^{-1}). Microhardness was measured using LM700AT (LECO) tester at a load of 0.025 kg.

3. RESULTS

3.1 Microstructure Characterization

Figure 1a illustrates the microstructure of the as-carburized specimen of a Ti-6Al-4V alloy. As seen, the inner layers consist of ($\alpha + \beta$) lamellae of dark contrast lying within the coarse grains of up to 600 μm in diameter. The superficial carburized layer is clearly distinguished by its white contrast pointing to its α-structure (a hexagonal-closed packed (HCP) lattice). It is formed due to the diffusion of carbon which stabilizes the single-phase α-structure [18]. The visually defined width of a carburized layer is varied from ~ 440 μm to 700 μm depending on the crystallographic orientation of the adjusted non-carburized grain. The carburized layer consists of three layers (Fig. 1a) with a specific structure: (i) next-to-surface layer of 75-100 μm width consisting of the small equiaxed grains, (ii) fine (5-10 μm wide) lamellae layer of 85-100 μm width, (iii) the layer formed by wide (10-50 μm) long epitaxial plates oriented nearly perpendicular to the surface (see insert to Fig. 1a). Also, the cracks propagating from the surface are observed within layers (i) and (ii) (shown by the arrow in Fig. 1a).

As follows from Fig. 1b, the laser processing led to the alteration of the specimen structure. The white-contrast carburized α-pattern (Fig. 1a) has evolved to the dark-contrast layer (heat affected zone - HAZ) with the long needles of α-martensite extended to a depth of about 0.8 mm (Fig.1b). On its very top, a near-surface layer of 60-120 μm width was noticed due to its dispersed structure and wavy contour of the free surface (the subsurface is shown by the arrow in the insert to Fig. 1b). The distinctive features of a near-surface layer are the multiple cracks and internal roundish cavities lying next to the surface (at a depth of 10-15 μm).

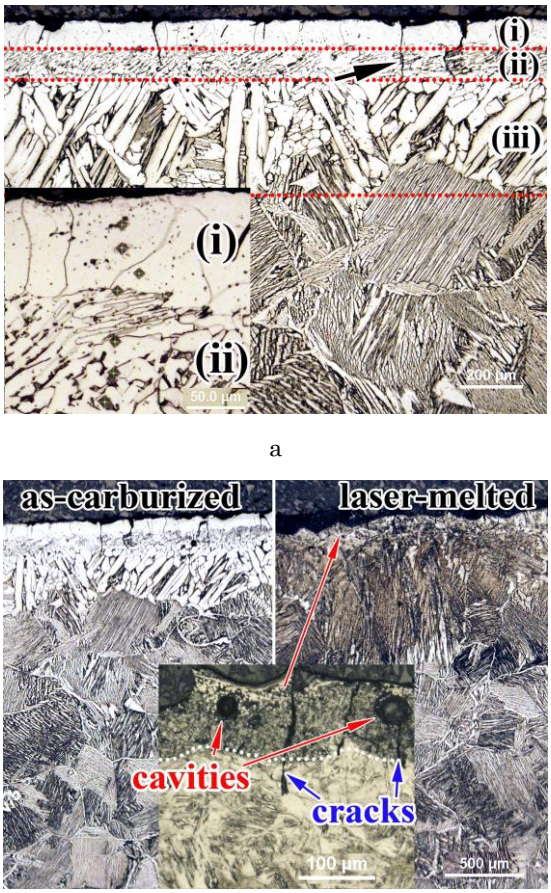

Fig. 1 – The OM images of cross-sectional microstructure of the specimens: (a) as-carburized state, (b) the alteration of a structure after the laser melting. (i, ii, iii are the layers within the carburized layer). (optical microscopy)

SEM observation was employed to reveal the structural peculiarities of a near-surface layer (both secondary electron (SEI) and back-scattered electron (BSE) modes were used). As seen in Fig. 2a, the rounded grooves appeared on the surface extending into the depths of 50 μm. The near-surface layer has a fine-grained structure with constituents of about 1-2 μm in diameter; fine short dendrites are also noted in the layer (shown in the insert to Fig. 1a). Near the surface the equiaxed angular inclusions of 1-5 μm in diameter are observed to a depth of up to 50 μm. The inclusions form the continuous chains or clusters of the conjunct particles (Fig. 2b). The particles feature the crystalline planes at an angle of about 60-65 degrees to each other. At a higher distance from the surface the dendrite-shaped inclusions are present along with the equiaxed particles. The dendrite had a layered structure which reflects the "layer-by-layer" growing; the layered pattern of the inclusion is noticed along the long axis of the dendrite with the layer thickness of 0.04-0.08 μm (see insert to Fig. 2d). According to the slightly darker BSE-contrast (the left side of Fig.2b), the inclusions are enriched with the element(s) with lower atomic number.

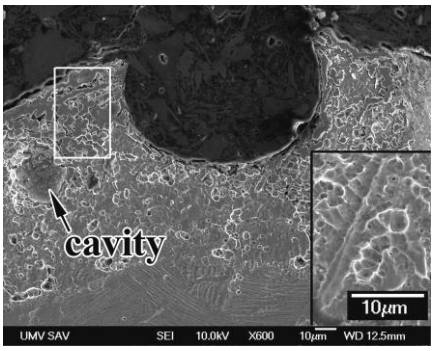

a

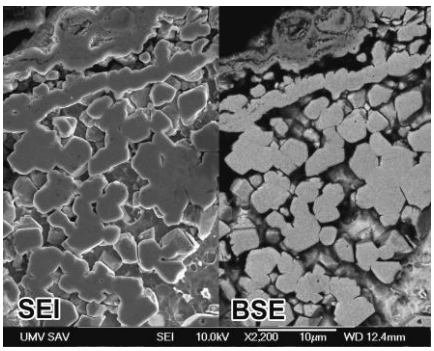

b

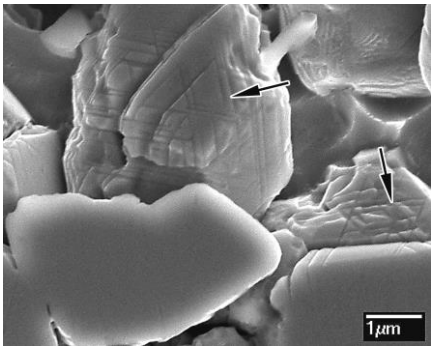

c

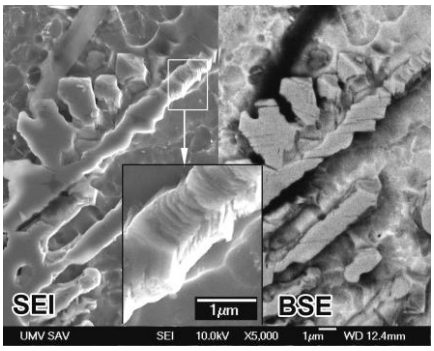

d

Fig. 2 – SEM images of microstructure of a near-surface layer in a laser-processed specimen: (a) the total view of the layer, (b) the enlarged area shown by the white rectangular in Fig. 1a (SEI and BSE images), (c) the crystalline planes in the particles, (d) the dendritic-shaped particles (SEI and BSE images)

3.2 XRD and EDS Characterizations

The results of the XRD study are depicted in Fig. 3. The XRD pattern of the as-carburized (oxidized) surface presents the peaks attributed to α-Ti, carbide TiC and oxides TiO_2 and Al_2O_3. According to the peak intensity carbide and oxide phases were predominant in the structure. After the oxidized (black) layer was gently polished-off, the XRD pattern "lost" the oxide/carbide peaks; only the ones for α-Ti remained (curve 2 in Fig. 3). This means that oxides and carbides were present in a very thin layer on the very top of the surface and they were removed under polishing. Curve 3 corresponds to the laser melted surface which was sand-blasted before the XRD study. As seen, even after removing the black oxidized layer, the peaks of carbide TiC and oxide TiO_2 again appeared in the XRD pattern along with α-Ti. The comparison of as-carburized and laser-melted patterns allowed to reveal that laser melting resulted in a shifting the peaks of α-Ti to the lower 2Teta angles reflecting much higher distortion of α-phase lattice in a laser-treated specimen.

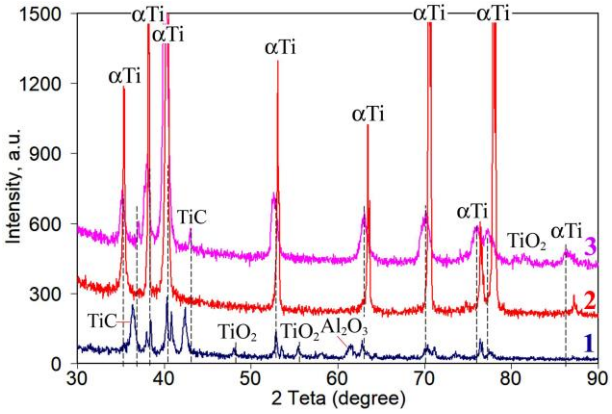

Fig. 3 – XRD patterns of LPBF Ti-6Al-4V alloy: 1 – as-carburized (oxidized), 2 – as-carburized (polished), 3 – laser-melted (sand-blasted)

The equiaxed angular inclusions (shown in Figs. 2b-d) contained (in average): 2.58 wt.% C, 0.55 wt.% Al, 14.25 wt.% O, 1.11 wt. % V, 81.80 wt. % Ti. The matrix next to inclusions (within the layer) contained much less carbon and oxygen: 1.60 % C, 9.54 wt.% O, 6.21 wt.% Al, 4.33 wt. % V, 78.32 wt.% Ti. The difference in chemical composition is illustrated by EDS-spectra (Fig. 4a and 4b respectively).

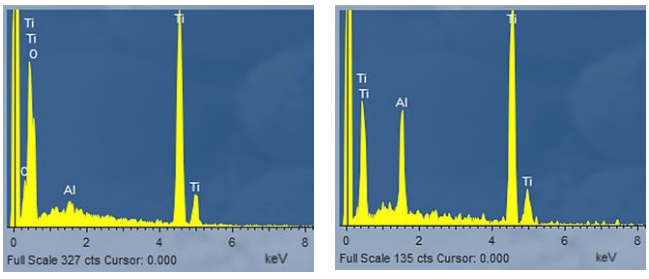

a b

Fig. 4 – EDS spectra of Ti-6Al-4V alloy: (a) angular particles in a laser-melted layer, (b) matrix in a laser-melted layer

3.3 Microhardness Measurements

The microhardness cross-section distribution is shown in Fig. 5. After carburizing the near-surface layer of 120 μm width had a microhardness of 720±12 HV. With distance from the surface, the microhardness gradually decreased according to the declining carbon content profile reaching 322±32 HV in non-carburized layers (at a distance of ≥0.7-0.8 mm). Thus, the carburized layer was two times harder as compared to the inner layers. It became even much harder after laser melting when microhardness increased up to 1000-1200 HV at a depth of less than 60 μm. At the depth of 120-150 μm the microhardness curves for carburized and laser-melted specimens practically overlapped. Thus, laser melting led to a 1.6 times and 3.5 times increase in microhardness relative to carburized and non-carburized states accordingly.

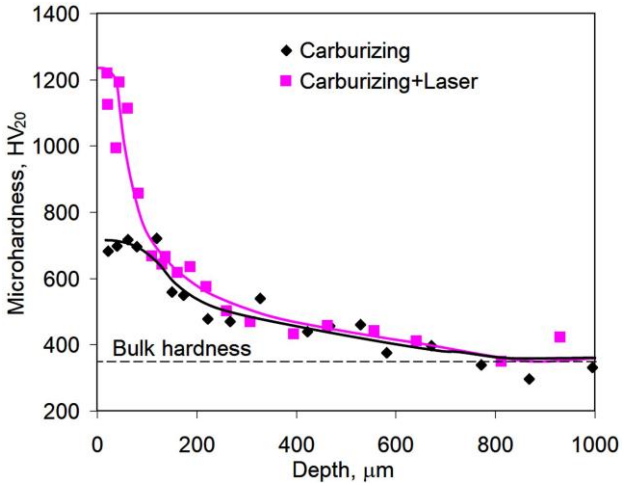

Fig. 5 – Microhardness profile in cross-section of carburized and laser-melted specimens of Ti-6Al-4V alloy

4. DUSCUSSION

According to the "Ti-C" phase diagram [18], carbon dissolves in the α-Ti increasing the $\alpha \leftrightarrow \beta$ transformation temperature. After exceeding the solubility threshold (2 at. %), carbon forms a δ-phase (titanium carbide TiC) with a structure of the NaCl type (Pearson symbol C.F8, space group Fm3m). This explains the nature of the change in the structure along the depth of the carburized layer: as follows from XRD pattern, titanium carbide and an α-phase were formed in a thin surface layer together with oxide phases TiO_2 and Al_2O_3 (the latter appeared at an earlier stage of carburization with the reaction of atmospheric oxygen inside the box). Beneath, a layer of carbon-stabilized alpha phase is located (layer (i) in Fig. 1a). Below in the structure, in addition to the α-Ti, β-Ti appears in the form of thin dark films lying along the boundaries of the α-phase plates (layers (ii) and (iii)). The plates in layer (iii) are located according to the direction of carbon atoms' diffusion deep into the sample. The layers (i) and (ii) contain cracks initiated by the tensile stress that occurred due to difference in a specific volume of α-structure in the carburized layer and $(\alpha + \beta)$ structure in the basis of the sample.

The laser melting led to the formation of two-zone surface layer consisting of a melting zone ((i) in Fig. 1b) and heat affected zone (ii) (HAZ). The depth of melting was not high (~ 100 μm on average) as compared with steels because of the low thermal conductivity of Ti-6Al-4V alloy (~ 15 $Wm^{-1}{\cdot}K^{-1}$) [19] which is about 1.7 times lower than that of, for example, 316L steel (~25 $Wm^{-1}{\cdot}K^{-1}$) [20] which has a laser melting depth of 200 μm (under the much lower heat input as compared with the present work: scan speed of 380 $mm{\cdot}sec^{-1}$, laser beam power of 105 W) [21]. The low thermal conductivity of Ti-6Al-4V alloy leads to overheating of the surface layers with its evaporation and ebullience resulting on the wavy surface (Fig. 2a) and low melting depth. Under melting, titanium interacted with carbon and atmospheric oxygen resulting in the formation of a complex phase containing Ti, O and C (as follows from EDS analysis) which can be acknowledged as titanium oxycarbide $Ti(O_{1-x}C_x)$. The presence of this phase in Ti-alloys was described by Miller et al. [22] which used the solid state reactions of TiO and TiC powders to synthesize the $Ti(O_{1-x}C_x)$ compound with a nominal composition of $Ti(O_{0.5}C_{0.5})$. The thermodynamic and structural studies of titanium oxycarbide were further performed by Jiang et al. [23, 24]. $Ti(O_{1-x}C_x)$ has the same Face-Centered-Cubic structure as that of TiC therefore it was identified in the XRD pattern as TiC. According to EDS results, the formula of oxycarbide can be presented as $Ti(O_{0.8}C_{0.2})$. It does not include V and Al (found in the oxycarbide) because of their low amounts which can be affected by (Al, V)-rich matrix surrounding the oxycarbide particles (the EDS-analyzed area is comparable to the particle size) [25].

As follows from SEM observations, titanium oxycarbide has the same angular morphology which is characteristic of titanium carbide. The similarity in chemical composition, morphology, and crystal lattice suggests one assume that $Ti(O_{1-x}C_x)$ is close to TiC in physical-mechanical properties (including hardness) [26]. Therefore, the presence of the dispersed inclusions of titanium oxycarbide in the melted layer can explain its extremely high hardness (1000-1200 HV). Another reason for such hardness is a modified matrix structure which is C-enriched αTi-martensite with a highly distorted lattice (the distortion is indicated by shifting of XRD peaks to lower angles). The distortion could be induced by an increase in lattice parameter (due to over-saturation with carbon) and by the accumulation of dislocation in the course of shear $\beta \rightarrow \alpha$ transformation under fast cooling (Fig. 3). Also, the fine-dendritic structure may contribute to the hardness of a melted layer employing a Hall-Petch effect. The formation of fine dendrites was due to the high cooling rate by heat removal deep into the sample. Refined dendrites increased the length of the internal surfaces which may pin the gliding dislocations thus strengthening the alloy.

Laser treatment allowed the quenching of a carburized layer to its full depth belonging to the heat-affected zone (Fig. 2b). The layer of C-rich α-martensite can server as a hard substrate which prevents a thin very hard layer from being punched through. This

should increase the bearing capacity of the laser-fused layer under contact loading.

The results obtained show that a carburizing with consecutive laser melting lead to advanced hardness of Ti-6Al-4V alloy due to formation of cermet layer and solid-solution strengthening of a *C*-stabilized α-phase. From this point of view, the above technology has prospects to improve a Ti-6Al-4V applicability for tribological applications [27]. However, it has some disadvantages the major of them is the deterioration of the surface condition, which is manifested in the appearance of multiple cracks and formation of a pronounced roughness. The latter is a result of the boiling of the molten pool under the laser beam. Another drawback is a formation of internal cavities inside the laser melted layer which are likely the shrink sinks resulted from fast crystallization. The resolving the above issues require further adjusting the parameters of a laser melting to comply the thermophysical characteristics of a particular titanium-based alloy.

CONCLUSIONS

The solid pack carburization and consecutive laser melting were applied to the LPBF-manufactured Ti-6Al-4V alloy. This allowed to synthesize an oxycarbide $Ti(O_{0.8}C_{0.2})$ in the form of equiaxed or dendrite-shaped particles lying within a 60-120 μm wide laser melted layer. This layer had an advanced (1000-1200 HV) hardness due to the presence of oxycarbide particles dispersed in the *C*-rich fine-dendritic αTi-martensite matrix. The *C*-rich HAZ layer beneath (needle-like αTi-martensite) extends to a depth of 0.8 mm with a gradual decrease in hardness from 1000 HV to 320 HV. The pack carburizing led to cracks emerging within the carbon-stabilized αTi layer. The subsequent laser melting led to a rough surface with an increased number of cracks as well as the formation of internal cavities in a sub-surface layer. Such a response of the Ti-6Al-4V alloy to laser melting is caused by surface overheating due to the low heat conductivity of the alloy.

ACKNOWLEDGMENTS

This research was supported by the Ministry of Education and Science of Ukraine (project No 0123U101834). V.G. Efremenko, Yu.G. Chabak and V.I. Zurnadzhy appreciate the support in the framework of the "EU Next Generation EU through the Recovery and Resilience Plan for Slovakia" under projects No. 09I03-03-V01-00061 and No. 09I03-03-V01-00099 respectively.

REFERENCES

1. V.S. de Viteri, E. Fuentes, *Titanium and Titanium Alloys as Biomaterials*, 154 (London: InTech: 2013).
2. Z.A. Duriagina, I.A. Lemishka, A.M. Trostianchyn, V.V. Kulyk, S.G. Shvachko, T.L. Tepla, E.I. Pleshakov, T.M. Kovbasyuk, *Powder Metall. Met. Ceram.* **57**, 697 (2019).
3. Y. Chabak, B. Efremenko, I. Petryshynets, V. Efremenko, A.G. Lekatou, V. Zurnadzhy, I. Bogomol, V. Fedun, K. Kovaľ, T. Pastukhova, Materials **14**, 7671 (2021).
4. Q. An, J. Chen, Z. Tao, W. Ming, M. Chen, *Int. J. Refract. Met. Hard Mater.* **86**, 105091 (2020).
5. B. Dong, X. Guo, K. Zhang, Y. Zhang, Z. Li, W. Wang, C. Cai, *Surf. Coat. Technol.* **429**, 127951 (2022).
6. M.A. Vasylyev, B.N. Mordyuk, V.P. Bevz, S.M. Voloshko, O.B. Mordiuk, *Int. J. Surf. Sci. Eng.* **14**, 1 (2020).
7. A.P. Burmak, S.M. Voloshko, B.M. Mordyuk, T.A. Krasovskyi, V.I. Zakiev, I.A. Vladymyrskyi, M.A. Vasylyev, *Metallofiz. Noveishie Tekhnol.* **44** No 11, 1453 (2022).
8. Z. Keresztes, D. Pammer, J.P. Szabo, *Period. Polytech., Mech. Eng.* **63** No 3, 195 (2019).
9. L.F. Sukhodub, L.B. Sukhodub, M.O. Kumeda, A.P. Denysenko, M.I. Kravchenko, *J. Nano- Electron. Phys.* **12** No 3, 03025 (2020)
10. J. Grabarczyk, J. Gaj, B. Pazik, W. Kaczorowski, B. Januszewicz, *Tribol. Int.* **153**, 106560 (2021).
11. Y. Luo, H. Jiang, G. Cheng, H. Liu, *J. Bionic Eng.* **8**, 86 (2011).
12. H. Duan, Yu. Han, W. Lu, J. Mao, L. Wang, D. Zhang, *Trans. Nonferrous Met. Soc. China* **26**, 1871 (2016).
13. Z. Zhao, P. Hui, T. Wang, X. Wang, Y. Xu, L. Zhong, M. Zhao, *J. Alloys Compd.* **745**, 637 (2018).
14. Y.-Z. Xing, C.-P. Jiang, J.-M. Hao, *Vacuum* **95**, 12 (2013).
15. X. Yazhe, J. Chaoping, H. Jianmin, *Rare Met. Mater. Eng.* **42** No 6, 1101 (2013).
16. Z.A. Duriagina, T.L. Tepla, V.V. Kulyk, R.Y. Kosarevych, V.V. Vira, O.A. Semeniuk, *J. Achiev. Mater. Manuf. Eng.* **93** No 1-2, 5 (2019).
17. T. Dong, P. Lu, Q. Ma, G. Li, Q. Liu, B. Fu, J. Li, *Surf. Coat. Technol.* **466**, 129608 (2023).
18. A.I. Gusev, Russ. Chem. Rev. **71**, 439 (2002).
19. M. Boivineau, C. Cagran, D. Doytier, V. Eyraud, M.H. Nadal, B. Wilthan, G. Pottlacher, *Int. J. Thermophys.* **27**, 507 (2006).
20. P. Pichler, B.J. Simonds, W. Jeffrey, G. Pottlacher, *J. Mater. Sci.* **55** No 9, 4081 (2020).
21. E. Yasa, J-P. Kruth, *Procedia Eng.***19**, 389 (2011).
22. D.N. Miller, A.K. Azad, H. Delpouve, L. Quazuguel, J. Zhou, A. Sinha, P. Wormalda, J.T.S. Irvine, *J. Mater. Chem. A* **4**, 5730 (2016).
23. B. Jiang, J. Xiao, K. Huang, J. Hou, S. Jiao, H. Zhu, *J. Am. Ceram. Soc.* **100** No 5, 2253 (2017).
24. B. Jiang, K. Huang, Z. Cao, H. Zhu, *Metall. Mater. Trans. A* **43**, 3510 (2012).
25. Y. Zhang, K. Shimizu, X. Yaer, K. Kusumoto, V.G. Efremenko, *Wear* **390-391**, 135 (2017).
26. O.V. Sukhova, V.A. Polonskyy, *East Eur. J. Phys.* **3**, 5 (2020).
27. Y. Chabak, V. Efremenko, V. Zurnadzhy, V. Puchý, I. Petryshynets, B. Efremenko, V. Fedun, K. Shimizu, I. Bogomol, V. Kulyk, D. Jakubéczyová, *Metals* **12**, 218 (2022).

Лазерне оплавлення навуглецевого біомедичного сплаву на основі титану, виготовленого методом LPBF-друку

Б.В. Єфременко[1], Ю.Г. Чабак[1,2], О.В. Цветкова[1], А.В. Джеренова[1], В.Г. Єфременко[1,2], Ф. Кромка[2], В.І. Зурнаджи[1,2], І.М. Олійник[1]

[1] *Приазовський державний технічний університет, вул. Університетська, 7, 87555 Маріуполь, Україна*
[2] *Institute of Materials Research, Slovak Academy of Sciences, 04001 Kosice, Slovakia*

Об'єктом даної роботи є дослідження зміни мікроструктури та твердості біомедичного сплаву Ti-6Al-4V, виготовленого за технологією LPBF-друку, в результаті цементації в твердому карбюризаторі та подальшого оплавлення поверхні лазерним променем. Навуглецювання проводили в порошковому карбюризаторі (20 об. % $(NH_2)_2CO$, 20 об. % $K_4Fe(CN)_6$ та 60 об. % сажі) при 1000 °C впродовж 7 год. Для лазерної обробки використали волоконний лазер «TruFiber 400» (TRUMPF) (довжина хвилі – 1064 нм, потужність – 400 Вт, швидкість сканування – 5 мм·с$^{-1}$). Дослідження включали оптичну (GX71 OLYMPUS) та скануальну електронну мікроскопію (JSM-7000F JEOL), енергодисперсійну спектроскопію (INCAx-sight, Oxford Instruments), рентгенівську дифракцію (X'Pert PRO, PANalytical, Cu-Kα) та вимірювання мікротвердості (LM700AT LECO, навантаження 0,05 кг). Було виявлено, що цементація забезпечила формування шару стабілізованої вуглецем αTi-фази товщиною 440-700 мкм з тонким верхнім шаром, що містить TiC, TiO_2 та Al_2O_3. Після навуглецювання твердість приповерхневого шару склала 720±12 HV, що вдвічі вище твердості основи (322±32 HV). Наступне сканування лазерним променем сформувало оплавлений шар товщиною 60-120 мкм, під яким на глибину до ~ 0,8 мм простяглася зона термічного впливу, що складалась із збагаченого на вуглець голчастого αTi-мартенситу. Оплавлений шар мав дрібнозернисту структуру, яка вміщувала дисперсні включення оксикарбіду $Ti(O_{0,8}C_{0,2})$ зернистої або дендритної форми. Твердість оплавленого шару становила 1000-1200 HV з подальшим поступовим зниженням вглиб зразка відповідно до зниження вмісту вуглецю. Лазерне оплавлення супроводжувалося утворенням тріщин і усадкових порожнин у приповерхневому шарі. Також воно призвело до підвищення шорсткості поверхні внаслідок її кипіння під лазерним променем, що пов'язано із низькою теплопровідністю сплаву Ti-6Al-4V.

Ключові слова: Біомедичний сплав на основі титану, Цементація, Лазерне плавлення, Мікроструктура, Мікротвердість.